Plasmonic Ag nanoparticles via environment-benign atmospheric microplasma electrochemistry

2013 Nanotechnology 24 095604

(http://iopscience.iop.org/0957-4484/24/9/095604)

Nanotechnology **24** (2013) 095604 (7pp) doi:10.1088/0957-4484/24/9/095604

Plasmonic Ag nanoparticles via environment-benign atmospheric microplasma electrochemistry

X Z Huang[1], X X Zhong[1], Y Lu[1], Y S Li[1], A E Rider[2,3], S A Furman[2] and K Ostrikov[2,3,4]

[1] Key Laboratory for Laser Plasmas (Ministry of Education) and Department of Physics, Shanghai Jiao Tong University, Shanghai 200240, People's Republic of China
[2] CSIRO Materials Science and Engineering, PO Box 218, Lindfield, New South Wales 2070, Australia
[3] Plasma Nanoscience @ Complex Systems, School of Physics, The University of Sydney, New South Wales 2006, Australia
[4] School of Physics and Advanced Materials, University of Technology Sydney, PO Box 123, Broadway New South Wales 2007, Australia

E-mail: xxzhong@sjtu.edu.cn

Received 5 November 2012, in final form 17 January 2013
Published 12 February 2013
Online at stacks.iop.org/Nano/24/095604

Abstract
Atmospheric-pressure microplasma-assisted electrochemistry was used to synthesize Ag nanoparticles (NPs) for plasmonic applications. It is shown that the size and dispersion of the nanoparticles can be controlled by variation of the microplasma-assisted electrochemical process parameters such as electrolyte concentration and temperature. Moreover, Ag NP synthesis is also achieved in the absence of a stabilizer, with additional control over the dispersion and NP formation possible. As the microplasma directly reduces Ag ions in solution, the incorporation of toxic reducing agents into the electrolytic solution is unnecessary, making this an environmentally friendly fabrication technique with strong potential for the design and growth of plasmonic nanostructures for a variety of applications. These experiments therefore link microplasma-assisted electrochemical synthesis parameters with plasmonic characteristics.

S Online supplementary data available from stacks.iop.org/Nano/24/095604/mmedia

(Some figures may appear in colour only in the online journal)

1. Introduction

Noble metal nanoparticles (NPs) are of immense interest in fields as wide ranging as plasmonics [1], biology [2], as well as catalysis [3]. Plasmonics (the study of plasmons, i.e. collective oscillations of valence electrons) in particular, is heavily reliant on noble metal nanomaterials, for applications from solar cells [4] to biosensors [5] to gene therapy [6, 7]. Of the plasmonic metals, Ag has been shown to be a promising material due to its anti-bacterial properties, high quality factor and plasmon resonance in the visible range [8–11]. One of the most important factors to control in Ag NP synthesis is the size and spacing of the NPs, which determine the resonance frequency in plasmonic applications [1].

Various methods have been used for the preparation of noble metal NPs, including chemical reduction [12–14] and more recently gas–liquid interface discharges or plasma–liquid electrochemistry (similar to glow discharge electrolysis, a plasma being a partially or completely ionized gas) [15–23]. Plasma–liquid electrochemistry involves a microplasma [24] coming into contact with an electrochemical cell and initiating reactions, be it either through direct reduction of aqueous ions [15, 22] or dissociation of water to form hydrogen radicals which then reduce the aqueous ions [24, 25]. The microplasma-assisted electrochemical

process is both particularly attractive for NP production and is environmentally and human health friendly as it does not involve any toxic reducing agents (e.g. sodium borohydride [26]). This method avoids the generation of undesired byproducts (as well as poor size/shape control as in the citrate method [27]) and affords a greater degree of control over the surface chemistry of the nanoparticles. Other production methods such as microwave [10] and ultrasound [11] also do not rely on the presence of a reducing agent.

Recent review articles [28, 29] have discussed the common background and similarities between gaseous plasmas and plasmonic phenomena. Plasmas also offer a reactive chemical environment in which to produce plasmonic nanoparticles. However, existing plasma electrochemistry reports on nanoparticle synthesis discuss plasmonic performance in a limited way [15, 22], but do not explicitly investigate the relationship of the microplasma-assisted electrochemical process parameters to plasmonic response. Such a parametric study is essential if the nanoparticles are to exhibit the desired plasmonic behaviour. This missing link is bridged in this paper.

Here, we examine both microplasma-assisted electrochemical synthesis of nanoparticles in a liquid and study their resultant plasmonic characteristics. We investigate the effect of the microplasma-assisted electrochemical process parameters such as the solution composition, the temperature of electrolyte, the presence of a stabilizer and whether or not the solution was stirred or agitated on Ag NP formation via microplasma-assisted electrochemistry. A strong link between the particle morphology and solution concentration/temperature is demonstrated via transmission electron microscopy (TEM) and ultraviolet–visible (UV–vis) spectroscopy, with particular attention paid to the location and characteristics of the plasmon resonance peak. We show that the nanoparticle size and spacing may be tuned by varying the microplasma-assisted electrochemical synthesis parameters, hence the plasmonic response of the nanoparticles may be controlled. This is an important experimental step towards bringing together plasma chemistry and plasmonics.

We will first present the experimental details, followed by a brief description of the results and then a comprehensive discussion of the formation mechanisms for the different experimental settings and the relevance to plasmonic applications. We will conclude with a summary of the study findings and an outlook for future research.

2. Experimental details

A Pt electrode (1 cm^2, 0.001 in thick, INESA Scientific Instrument Co., Ltd) was placed inside a reaction cell containing an electrolyte consisting of $AgNO_3$ (ranging from 0.1 to 1 mM, Shanghai Lingfeng Chemical Reagent Co. Ltd) and fructose ($C_6H_{12}O_6$, a common 'green' stabilizer to prevent uncontrolled growth and agglomeration, ranging from 0 to 0.05 mM, Sinopharm Chemical Reagent Co. Ltd) in de-ionized water. The silver nitrate dissociates in water to silver ions and nitrate ions: $AgNO_3 \rightarrow Ag^+ + NO_3^-$. A stainless steel capillary tube (175 μm inside diameter, 10 cm length, Unimicro Technologies Inc.) was placed 3 cm away from the Pt foil with a gap of 2 mm between the end of the tube and the reaction volume. Helium gas flow was coupled to the capillary tube and set to 25 sccm. The capillary tube acted as the cathode and the Pt foil as the anode, with a negatively biased dc power supply used [15] (the reaction vessel had an inner diameter of 6 cm). A high voltage of ∼2 kV was applied to ignite the microplasma.

Following gas breakdown (typically when the electric field strength reaches 10^7 V m^{-1}), the discharge current was kept constant, controlled by a DC current source. All of the experiments were carried out in a 10 ml reaction volume with a process time of 15 min and current of 3 mA. Unless noted otherwise, the electrolyte temperature was 25 °C. Later, the temperature was measured and controlled as follows: the electrolytic solution was placed in a cell, which was then put in a water bath (unheated in the 25 °C case, heated in the 70 °C case). The systems were allowed to come to thermal equilibrium, whereupon the water's temperature was then measured. UV–vis absorbance spectroscopy (dual channel fibre optic spectrometer (Avaspec-2048-2-USB2) with a balanced deuterium-halogen light source (AvaLight-DH-S-BAL)) was used to characterize the interaction of the Ag NPs with light. Particular attention was paid to plasmonic behaviour, hence the background spectrum from de-ionized water was subtracted from the plotted data [15], so the spectral features indicative of the silver nanoparticle could be more clearly observed and analysed. As-grown Ag NPs were then drop-cast on carbon-coated copper TEM grids and dried in air, for size and morphology analysis via TEM (JEM-2100F, using an accelerating voltage of 200 kV). In the absence of a stabilizer, the effect of stirring the solution on particle growth was also investigated.

3. Results

Here, we will first present the effect of solution concentration and operation temperature on the microplasma-assisted synthesis (see figure 1) of colloidal Ag NPs in the presence of a fructose stabilizer through TEM analysis and UV–vis absorption spectroscopy. We will then investigate the effects of solution concentration, both with and without stirring on the microplasma-assisted synthesis of Ag NPs without using a stabilizer. Particular attention will be paid to the size uniformity, dispersion and morphological structure of the Ag NPs.

Figure 2 plots the UV–vis absorbance spectra of Ag colloids with varied solution concentrations (the ratio of $AgNO_3$:fructose was set to 0.02, but the respective amounts added to the de-ionized H_2O were as follows: $AgNO_3$/fructose considered are 1 mM/0.05 M, 0.5 mM/0.025 M; 0.2 mM/0.01 M; 0.1 mM/0.005 M). As the concentration of $AgNO_3$ is increased, the peak position shifts noticeably to the red (i.e. from 402 nm to 420 nm as concentration is increased). This response is consistent with classical Mie theory which states that larger particles exhibit a red-shifted absorbance peak, which indicates that

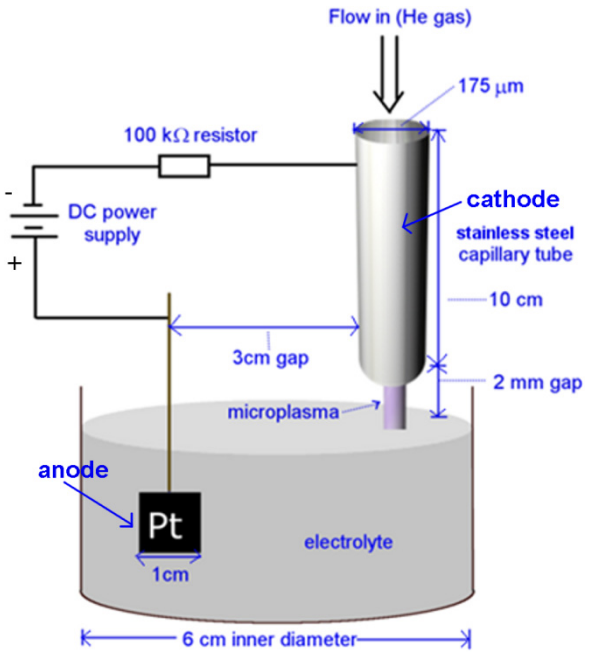

Figure 1. Schematic of electrochemical cell with an atmospheric-pressure He microplasma cathode and a Pt foil anode immersed in a $AgNO_3$/fructose/de-ionized water solution.

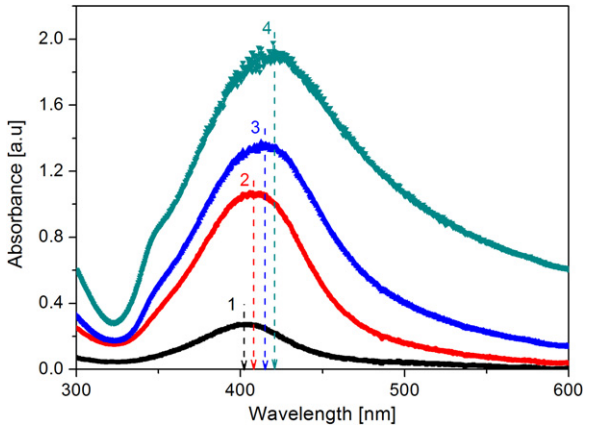

Figure 2. The effect of varying the $AgNO_3$ and fructose content in the electrolyte solution on the UV–vis absorbance spectra of Ag NPs produced via microplasma-assisted electrochemical synthesis, where $AgNO_3$ and fructose are: 1 = 0.1 mM and 0.005 M, 2 = 0.2 mM and 0.01 M, 3 = 0.5 mM and 0.025 M, 4 = 1.0 mM and 0.05 M.

the Ag NPs obtained via increased $AgNO_3$ concentrations are (on average) larger than the Ag NPs in the lower $AgNO_3$ concentration case. The increased peak intensity with higher $AgNO_3$ concentrations also suggests that more Ag NPs are produced in the high concentration case. Moreover, the broader absorption peaks (the full width at half maximum (FWHM) increases from 71 nm to approximately 133 nm; see supplementary data (SD) available at stacks.iop.org/Nano/24/095604/mmedia) with increased temperature suggest that the higher concentrations of $AgNO_3$ and fructose result in a broader size distribution of Ag NPs.

Figure 3 presents supporting TEM images of Ag NPs produced using $AgNO_3$/fructose concentrations of

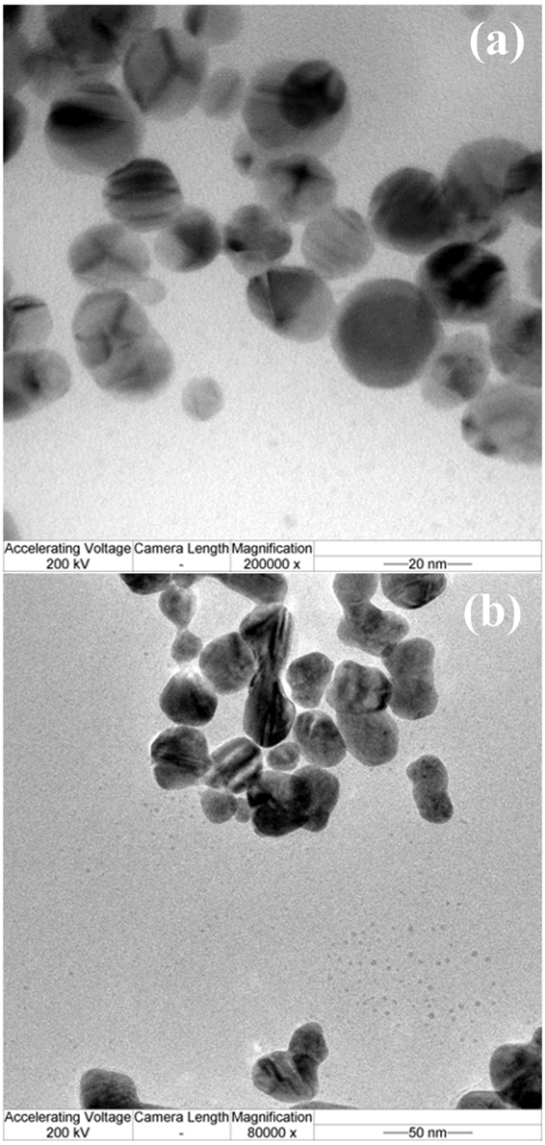

Figure 3. TEM images of Ag NPs synthesized by the microplasma-assisted electrochemistry method with silver salt and fructose contents of (a) $AgNO_3$ 0.2 mM and fructose 0.01 M, (b) $AgNO_3$ 1 mM and fructose 0.05 M.

(a) 0.2 mM/0.01 M and (b) 1 mM/0.05 M, henceforth 'low' and 'high' concentrations. For the 'low' concentrations in (a), we observe dispersive Ag NPs with diameters of 10–20 nm, whereas for the 'high' concentrations we observe Ag NP with diameters between 15 and 40 nm, with some evidence of coalescence. These findings are in line with the observed red shift with higher concentrations presented in the UV–vis absorbance spectroscopy results. A discussion of these findings and the implication of the broader absorption peak and possible coalescence of NPs with higher concentrations will be included in section 4.

Figure 4 presents the UV–vis absorption spectra of Ag colloids produced by the microplasma–liquid electrochemistry method using 0.2 mM $AgNO_3$ and 0.01 M fructose, with the electrolyte maintained at both room temperature (25 °C) and high temperature (70 °C). The spectra show a

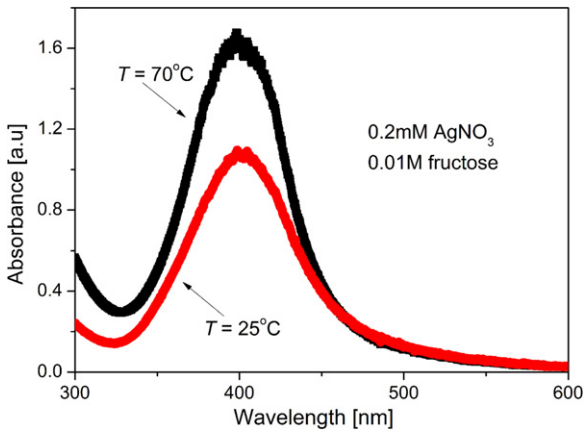

Figure 4. UV–vis absorbance spectra of Ag NPs produced via the microplasma-assisted electrochemistry method from an electrolyte solution (0.2 mM $AgNO_3$ and 0.01 M fructose) at temperatures of 25 and 70 °C.

higher absorbance (larger peak area) for the 70 °C case, which implies higher production efficiency for higher temperatures. The locations of the peak for the 25 and 70 °C cases are very close (402 nm and 399 nm, respectively) which indicates that the average size of the nanoparticles is approximately the same. However, the narrower FWHM for the 70 °C (71 nm) compared to a FWHM of 77 nm for the 25 °C case implies that the higher temperatures result in slightly more size-uniform NPs. Whilst a very subtle blue shift (by approximately 3 nm) is observed with the increased temperature, further focused investigation is required.

The TEM images from both the 25 °C and 70 °C cases are presented in figures 5(a) and (b), respectively. Whilst both images reveal Ag NP that are approximately spherical, ranging between 10 and 20 nm with an average diameter of about 15 nm, discrete and uniform, the 70 °C case is shown to exhibit greater NP dispersity. These findings are in good agreement with the results deduced from UV–vis absorbance spectroscopy. The production of Ag NPs without fructose as a stabilizer will be examined in figures 6 and 7. The concentration of $AgNO_3$ was varied from 2 to 4 and then to 8 mM. The corresponding UV–vis absorption spectra of the Ag NPs produced at room temperature both without and with stirring of the electrolyte are shown in figures 6(a) and (b), respectively. Figure 6(a) shows that as $AgNO_3$ concentration is increased, the intensity of the absorbance peak also increases. This indicates that more Ag NPs are produced with greater $AgNO_3$ concentration. The absorbance peak, although relatively broad (indicating a fairly non-uniform size distribution), appears to be centred around the same value for all three concentrations considered (approximately 435 nm), which indicates that there is not a marked influence exerted by solution concentration on the average NP size produced. The same concentrations are considered in figure 6(b), albeit with stirring incorporated. Here, the UV–vis spectra display roughly the same behaviour with silver nitrate concentration (peak location is approximately 420 nm for all three concentrations). However, the increased peak area indicates that more Ag NPs are produced with stirring.

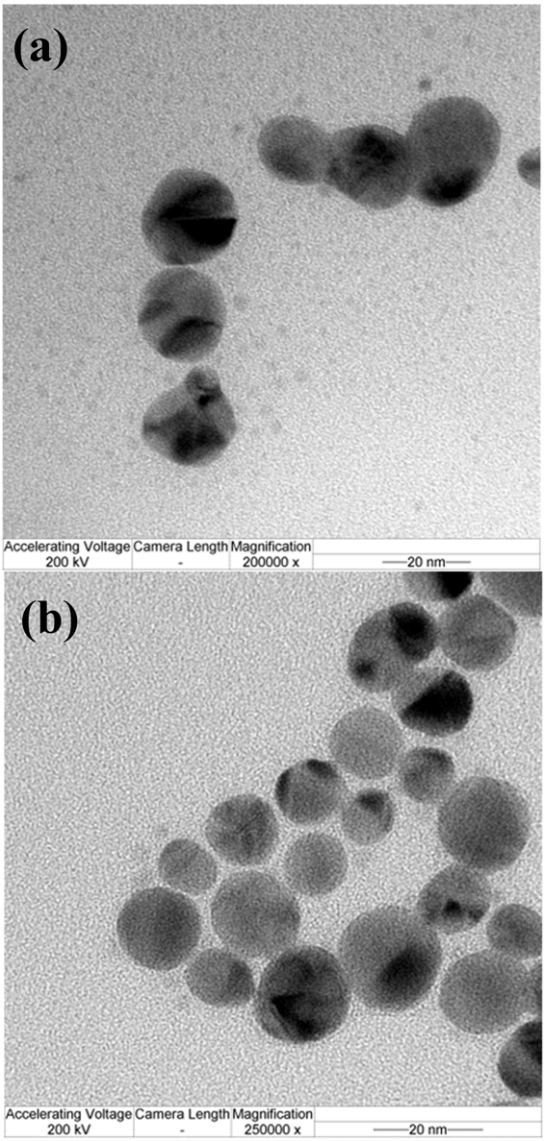

Figure 5. TEM images of Ag NPs synthesized at temperatures of 25 °C (a) and 70 °C (b) via the microplasma-assisted electrochemistry method.

The corresponding TEMs for the cases considered in figure 6 are presented in figures 7(a) and (b), respectively. From visual inspection of (a), it is clear that without stirring, the stabilizer-free method results largely in non-uniform sized (between 5 and 35 nm), agglomerated particles of an undefined, irregular shape. The particles produced via the stabilizer-free method incorporating stirring in figure 7(b), by comparison, are seen to be spherical, disperse and have a better size uniformity (10–25 nm). Further discussion of this behaviour will be presented in section 4.

4. Discussion

4.1. Factors influencing Ag NP formation

A few microplasma-assisted electrochemical process parameters influencing Ag NP formation via microplasma-assisted

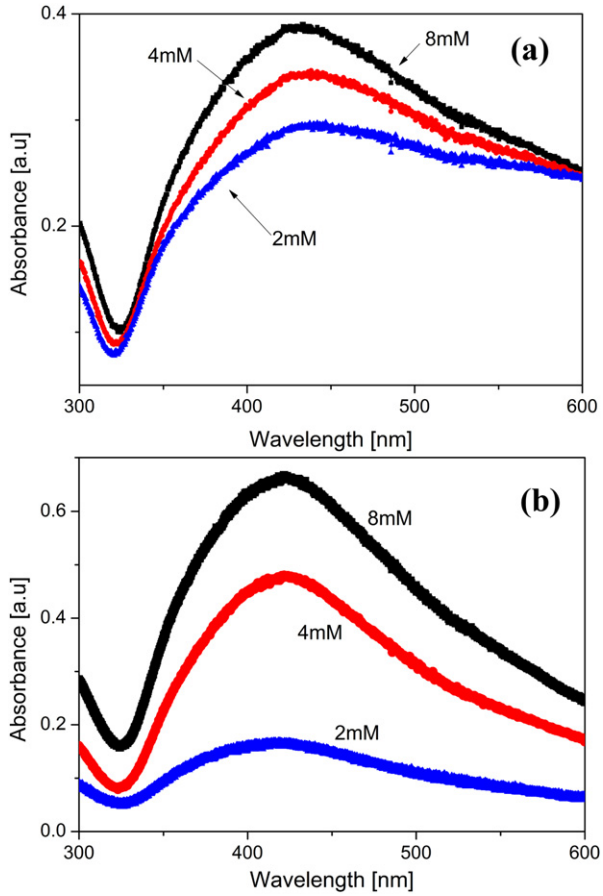

Figure 6. UV–vis absorbance spectra of Ag NPs synthesized by the stabilizer-free microplasma-assisted electrochemistry method with varied $AgNO_3$ concentration (a) without stirring and (b) with stirring.

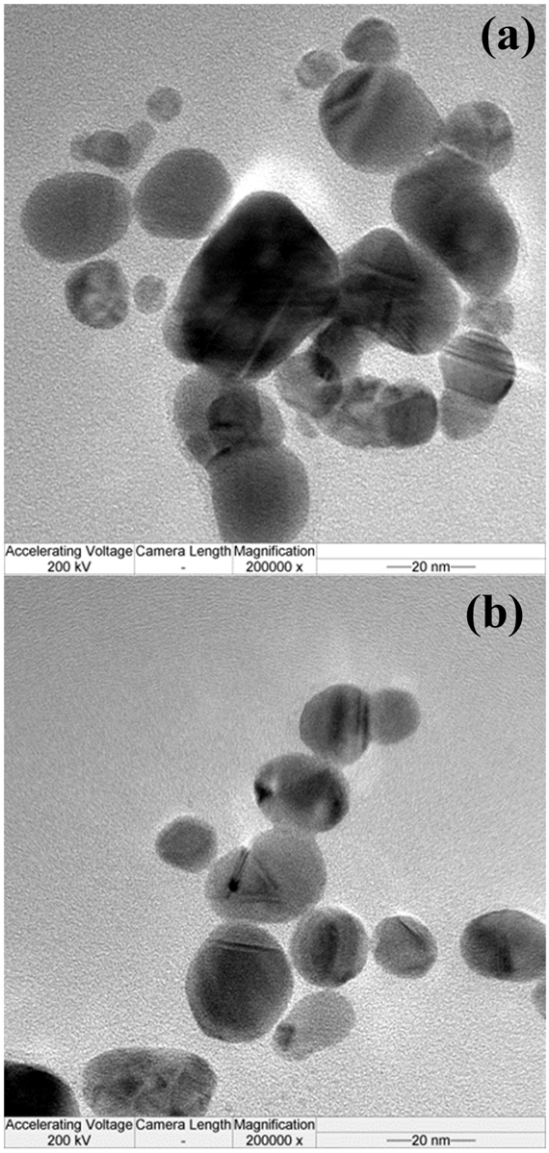

Figure 7. TEM images of Ag NPs synthesized by the stabilizer-free microplasma-assisted electrochemistry method with 4 mM $AgNO_3$ concentration (a) without and (b) with stirring.

electrochemistry were considered in this study, namely the solution composition, the temperature of electrolyte, the presence of a stabilizer and whether the solution was stirred or left unagitated. Here we will discuss these factors in greater detail, paying attention to phenomenological changes as well as theoretical models.

When the microplasma touches the solution, energetic ions, radicals and electrons are delivered to the plasma–liquid interface which leads to the silver ions in solution being reduced ($Ag^+ + e^- \rightarrow Ag$). In liquid–plasma electrochemistry, electron-induced reactions are the predominant reaction path [30]. After a few minutes, a yellowish colour in the immediate vicinity of the microplasma indicates the growth of colloidal metal NPs, which are then coated with fructose (if present). As time passes, these Ag NPs diffuse into the greater solution, as expected from Brownian motion; this is confirmed by the gradual colour change of the solution, from colourless to yellowish to yellow. When the concentration of $AgNO_3$ is increased, more nanoparticles are produced. This is logical, as more Ag ions are available to be reduced by the plasma-generated electrons and subsequently agglomerate into Ag nanoparticles.

Whilst we focused on a fixed $AgNO_3$/fructose ratio in this paper, we expect that increasing the amount of fructose relative to $AgNO_3$ would result in a larger number of smaller NPs (weaker agglomeration, NP growth is limited earlier due to large amounts of stabilizer). There is the additional possibility that it would also increase the reduction of the silver ions in the greater bulk of the solution, rather than just in the locality of the microplasma. This is because in addition to acting as a stabilizer (i.e. limiting the agglomeration of colloidal nanoparticles), fructose can also act as a reducing agent, leading to the following reaction: $2Ag^+ + C_6H_{12}O_6 + H_2O \rightarrow 2Ag + C_6H_{12}O_7 + 2H^+$ [31]. However, given the higher energy of the plasma-generated electrons versus electrons generated in solution as a result of standard redox reactions, we expect that the greatest reduction of Ag ions would still occur in the locality of the microplasma. Care should also be taken as using fructose during synthesis can lead to interference with the signals from chemical species

if the Ag NPs are to be used as a surface-enhanced Raman scattering (SERS) probe [22].

When the temperature was increased, the colour in the immediate vicinity of the microplasma changed more quickly and diffused throughout the greater solution more rapidly. To explain this, we use the Stokes–Einstein equation for the diffusion coefficient of the nanoparticles in solution [32]:

$$D_{iB}^{\infty} \approx \frac{kT}{6\pi \eta_B r_i}, \tag{1}$$

where k is the Boltzmann constant, T is the temperature of the liquid, η_B is the viscosity of the fluid and r_i is the radius of the Ag particles. From (1) it follows that when temperature is increased, the particles have a higher diffusion coefficient (as temperature is changed from 25 to 70 °C, according to equation (1), the diffusion coefficient should increase by a factor of 2.8, assuming everything else remains the same). This also can be linked to the dispersion of the nanoparticles. Indeed, it is clear from figure 5(b) that at higher temperature, more NPs are produced (verified by the more intense absorbance peak in figure 4) and they are more dispersed (i.e. there is a greater interparticle spacing in the solution). It is expected that a higher temperature will also increase the reaction rate and hence production of Ag NPs.

Regarding the role of the microplasma [24] in NP formation, it was suggested [22] that the Ag NP size is largely controlled by the elementary processes in the region immediately adjacent to the microplasma. This is a reasonable assumption when considering the higher energy of the plasma-generated electrons versus electrons generated in solution as a result of standard redox reactions. This interpretation is supported by the more size-uniform NPs obtained in the stabilizer-free case when stirring was incorporated as opposed to when the solution remained unagitated (see figure 6)—the stirring led to faster NP diffusion away from the plasma region.

Regarding the explicit variation of microplasma parameters: we expect that by increasing current (and processing time), more plasma-electrons would be available to reduce Ag ions. This would lead to greater reduction of Ag ions (due to increased availability of energetic electrons), hence more nucleation sites and higher NP growth rates. We would expect more particles to be produced with increased current, but it would not necessarily influence the average particle size. Whilst we visually observe initial nanoparticle formation around the liquid–plasma interface (indirectly, via the colour change in the solution) when the microplasma is operating, the NPs then diffuse into the greater solution. There the NPs may continue to grow until they are 'capped' by a stabilizer or agglomerate. There is no evidence to say that the growth stops when the NP leaves the liquid–plasma interface. Chiang *et al* [33], in a similar investigation, noted that increasing discharge current and processing time led to increased particle agglomeration and larger growth rates, but did not appreciably affect the particle size.

4.2. Plasmonic effects

Given the approximately spherical nature of the nanoparticles, Mie theory may be used as a first approximation to describe the interaction of the Ag colloids with light. The extinction coefficient, C_{ext}, may be written as [1]:

$$C_{ext} = \frac{24\pi^2 R^3 \varepsilon_m^{3/2}}{\lambda}\left[\frac{\varepsilon_i}{(\varepsilon_r + 2\varepsilon_m)^2 + \varepsilon_i^2}\right], \tag{2}$$

where R is the radius of the NP, ε_m is the dielectric constant of the medium, λ is the excitation wavelength, and ε_i and ε_r are the imaginary and real parts of the complex dielectric constant for Ag, which may be expressed as:

$$\varepsilon_i = \frac{\omega_p^2 \nu_d}{\omega(\omega^2 + \nu_d^2)}, \qquad \varepsilon_r = \varepsilon^{\infty} - \frac{\omega_p^2}{\omega(\omega + \nu_d^2)},$$

respectively [34]. Here, ω_p and ν_d are the plasma and damping frequencies, respectively, ε^{∞} (between 4.7 and 5.9) is the high-frequency dielectric constant of Ag due to interband and core transitions [34].

The optical properties of Ag NPs are quite well established in the literature. What complicates analysis of the optical properties in this case is the role of the surrounding solution (i.e. comprised of fructose and water) described by the dielectric constant of the medium, ε_m, which can be approximated by applying the Landau–Lifshitz formula [35]:

$$\varepsilon_m^{1/3} = (1 - V)\varepsilon_A^{1/3} + V\varepsilon_B^{1/3}, \tag{3}$$

where V is the fraction by volume of the fructose, ε_A and ε_B are the dielectric constants of the fructose and water solution, and of the $AgNO_3$, respectively. The small concentrations (paired with a low $\varepsilon_r \sim 9.0$ [36]) of $AgNO_3$, mean that it will have a negligible effect on (3), compared to fructose and water (see SD for more details) and, indeed, to just plain water itself. Thus, a simple, qualitative way of looking at this is via the resonance condition for localized surface plasmons, from (2) we can see that ε_r needs to be close to $-2\varepsilon_m$ for resonance [1]. Thus, as ε_m increases, for resonance to be satisfied, ε_r will also have to increase. Based on available data [1] on ε_r for Ag, as ε_r increases, the wavelength of the resonant excitation decreases. Thus, considering the effect that increasing the mass fraction of fructose in the solution will reduce ε_m [37], we could extrapolate that removing fructose from the solution should increase the Ag NP size (supported by the increased peak resonance wavelength value in the UV–vis spectra in figures 2 and 6).

This influence of the surrounding medium is clear in the difference in the peak positions in the case of fructose versus no fructose. As the amount of fructose (and the corresponding amount of $AgNO_3$) was reduced in figure 2, the resonance peak shifted from 402 nm to 420 nm, whereas when no fructose was present in figures 6(a) and (b), the peak wavelength remained constant at 435 and 420 nm, for no stirring and stirring respectively—despite a fairly large change in the $AgNO_3$ concentration (from 2 to 8 mM). This suggests that in the case of microplasma-assisted electrochemical synthesis of AgNPs, the presence of a stabilizer is not essential. Indeed, as noted by Chang *et al* [22] in the case of microplasma-synthesized Ag NPs in SERS applications, the presence of a stabilizer can adversely interfere with the signal from the probe molecule. Whilst the peaks in the no stabilizer

case are broader and not as sharp as in the $AgNO_3$/fructose case, there is still an acceptable degree of size uniformity throughout, and a more constant maximum peak value. It is expected that by varying the microplasma parameters [38], the sharpness of the plasmon resonance peak may be improved. This will be the subject of future experiments.

5. Conclusions

The intersection of reactive plasma chemistry and plasmonics, in general, is a particularly interesting research area [28, 29]. In this paper, we investigated the microplasma-assisted electrochemical synthesis of Ag NPs. In particular, we showed that the nanoparticle size and interparticle spacing throughout the solution may be tuned by varying the microplasma-assisted electrochemical synthesis parameters, hence the plasmonic response may be controlled. It is clear that higher temperatures and solution concentrations result in highly dispersive Ag nanoparticles of larger sizes. We further demonstrate the fabrication of Ag nanoparticles without a stabilizer (beneficial for sensing as stabilizers can often interfere with the signal from the probe molecule). The UV–vis results were explained with reference to both plasmonics (specifically plasmon resonance and peak shifts) and microplasmas. This is an important experimental step towards bringing together plasma chemistry and plasmonics. These results are of practical importance for plasmonic applications such as sensing where the control of the nanoparticle characteristics is paramount.

Acknowledgments

XZH, XXZ, YL and YSL acknowledge support from the National Science Foundation of China (Grant No. 11275127, 90923005), Shanghai Science and Technology Committee (Grant No. 09ZR1414600), and the National ITER Plans Program of China (Grant No. 2009GB105000). KO acknowledges support from the Australian Research Council and the CSIRO OCE Science Leadership Scheme. AER acknowledges support from the CSIRO Sensors and Sensor Networks TCP and the CSIRO OCE Postdoctoral Fellowship Scheme.

References

[1] Rycenga M, Cobley C M, Zeng J, Li W, Moran C H, Zhang Q, Qin D and Xia Y 2011 *Chem. Rev.* **111** 3669
[2] Jain P, Huang X, El-Sayed I and El-Sayed M 2007 *Plasmonics* **2** 107
[3] Crooks R M, Zhao M, Sun L, Chechik V and Yeung L K 2011 *Acc. Chem. Res.* **34** 181
[4] Akimov Yu A and Koh W S 2010 *Nanotechnology* **21** 235201
[5] Mayer K M and Hafner J H 2011 *Chem. Rev.* **111** 3828
[6] Daniel M-C and Astruc D 2004 *Chem. Rev.* **104** 293
[7] Hatakeyama R and Kaneko T 2011 *Plasma Fusion Res.* **6** 1106011
[8] Blaber M G, Arnold M D and Ford M J 2010 *J. Phys.: Condens. Matter* **22** 143201
[9] Arnold M D and Blaber M G 2009 *Opt. Express* **17** 3835
[10] Schrand A M, Braydich-Stolle L K, Schlager J J, Dai L and Hussain S M 2008 *Nanotechnology* **19** 235104
[11] Oates T W H and Mücklich A 2005 *Nanotechnology* **16** 2606
[12] Jana N R and Peng X 2003 *J. Am. Chem. Soc.* **125** 14280
[13] Schulz-Dobrick M, Vijaya Sarathy K and Jansen M 2005 *J. Am. Chem. Soc.* **127** 12816
[14] Siekkinen A R, McLellan J M, Chen J and Xia Y 2006 *Chem. Phys. Lett.* **432** 491
[15] Richmonds C and Sankaran R M 2008 *Appl. Phys. Lett.* **93** 131501
[16] Furuya K, Hirowatari Y, Ishioka T and Harata A 2007 *Chem. Lett.* **36** 1088
[17] Baba K, Kaneko T and Hatakeyama R 2009 *Appl. Phys. Express* **2** 035006
[18] Baba K, Kaneko T and Hatakeyama R 2007 *Appl. Phys. Lett.* **90** 201501
[19] Baba K, Okada T, Kaneko T and Hatakeyama R 2006 *Japan. J. Appl. Phys.* **45** 8286
[20] Mallin M P and Murphy C J 2002 *Nano Lett.* **2** 1235
[21] Baba K, Okada T, Kaneko T, Hatakeyama R and Yoshiki H 2007 *Thin Solid Films* **515** 4308
[22] Chang F-C, Richmonds C and Sankaran R M 2010 *J. Vac. Sci. Technol.* A **28** L5
[23] Chiang W-H, Cochey M, Virnelson R C and Sankaran R M 2007 *Appl. Phys. Lett.* **91** 021501
[24] Mariotti D and Sankaran R M 2011 *J. Phys. D: Appl. Phys.* **44** 174023
[25] Koo I G, Lee M S, Shim J H, Ahn J H and Lee W M 2005 *J. Mater. Chem.* **15** 4125
[26] Yuan X, Yeow T J, Zhang Q, Lee J Y and Xie J 2012 *Nanoscale* **4** 1968
[27] Pillai Z S and Kamat P V 2004 *J. Phys. Chem.* B **108** 945–51
[28] Rider A E, Ostrikov K and Furman S A 2012 *Eur. J. Phys.* D **66** 226
[29] Wang Y, Plummer E W and Kempa K 2011 *Adv. Phys.* **60** 799
[30] Mariotti D, Patel J, Svrcek V and Maguire P 2012 *Plasma Proc. Polym.* **9** 1074
[31] Dehanavi A S, Raisi A and Aroujalian A 2013 *Synth. React. Inorgan., Met.-Organ., Nano-Met. Chem.* at press
[32] Levine I N 2002 *Physical Chemistry* 5th edn (New York: McGraw-Hill)
[33] Chiang W-H, Richmonds C and Sankaran R M 2010 *Plasma Sources Sci. Technol.* **19** 034011
[34] Mulvaney P 1996 *Langmuir* **12** 788
[35] Shin F G, Tsui W L and Yip M Y 1992 *J. Mater. Sci. Lett.* **11** 132
[36] Haynes W M (ed) 2012 Permittivity (dielectric constant) of inorganic solids *CRC Handbook of Chemistry and Physics* 92nd edn (Boca Raton, FL: Chemical Rubber Company (CRC Press)/Taylor and Francis) Internet Version
[37] Hernández-Luis F, Grandoso D and Lemus M 2004 *J. Chem. Eng. Data* **49** 668
[38] Richmonds C, Witzke M, Bartling B, Lee S W, Wainright J, Liu C-C and Sankaran R M 2011 *J. Am. Chem. Soc.* **133** 17582